

Transient approximated Green's Function of a circular line source on a half space for fast simulation of axisymmetric problems

Mario Wolf
Institute of Solid State Electronics
Technische Universität Dresden
Dresden, Germany
mario.wolf@tu-dresden.de

Elfgard Kühnicke
Institute of Solid State Electronics
Technische Universität Dresden
Dresden, Germany
elfgard.kuehnicke@tu-dresden.de

Abstract— Half-analytical methods are an efficient way to model the sound propagation. Conventionally, they are based on integral transform methods, where the wave equation is solved for a point source. Extended sources are generated by covering the active area with point sources and superposing their fields. For radial symmetric problems, the calculation effort can be reduced significantly by covering the active area with ring sources. The solution of the wave equation for a ring-like excitation is only known in the transformed domain. This contribution presents a new approach calculating Green's function for a ring-like excitation by transferring approximated harmonic Green's functions into time domain. The method is evaluated by comparing it with the emission of disc shaped source. As an example the method is applied to determine the uncertainty for measuring the sound velocity in tissue phantoms, is presented.

Keywords—transient modelling, axial symmetry, Green's functions, sound velocity measurement, uncertainty

I. INTRODUCTION

New ultrasound techniques work by evaluating additional sound field parameters besides time of flight. The development of such techniques requires sound field calculations to optimize probe parameters and to define evaluation criteria. There are methods to calculate the time harmonic sound field by means of Green's functions combined with separation method and point source synthesis [1]. The transient sound field, e.g. echo signals for a high number of reflector positions, is calculated by harmonic synthesis [2]. Since the axisymmetric structure of applied pre-focused annular-arrays, the use of ring sources instead of point sources at the interface between two half-spaces would reduce the calculation effort. Unfortunately, Green's functions for ring sources are well known only for the transformed domain [3].

In this contribution, it is shown that the usual routine using a steepest descent approximation for the inverse transform fails for Greens functions of ring sources on the interface of a half-space. Utilizing an approximated harmonic Greens function of a point source acting at the surface of a half- space, the field of the ring source can be obtained by a spatial convolution with the ring, which results in an integration over the angular coordinate.

This integral is evaluated by transforming the integral into time domain and applying the properties of Dirac delta function. An approximated transient Greens function for a ring source is derived. For validation, the transient wave emitted by a disc-shaped source is calculated by covering the disc with ring sources and superimposing the fields of all ring sources. Although surface waves are neglected, the signal-part of the longitudinal wave is in good agreement with an exact calculation by means of generalized ray theory using space convolution to the distribution of point sources.

By means of calculated sound fields the focusing range, the extension of the focus area and the signals are discussed. As an example, the algorithm is used to determine the uncertainty of locally resolved measurements of sound velocity in tissue phantoms.

II. DERIVATION OF GREEN'S FUNCTIONS

Axial-symmetric problems are described by the wave equation in cylinder coordinates for the potential Φ (eq. 1). To reduce the degree of equation, the Fourier transform and the Hankel transform, based on Bessel functions, is applied and yields to equation 2.

$$\frac{\partial^2}{\partial r^2} \Phi + \frac{1}{r} \frac{\partial}{\partial r} \Phi + \frac{\partial^2}{\partial z^2} - \frac{1}{c_L^2} \frac{\partial^2}{\partial t^2} \Phi = 0 \quad (1)$$

$$\frac{\partial^2}{\partial z^2} \Phi^{H_0} + (\xi^2 + k^2) \Phi^{H_0} = 0 \quad (2)$$

This equation can be solved by a conventional exponential ansatz. The constants of integration are determined by applying the boundary conditions. For point source synthesis a normal force is assumed at the coordinate origin (normal stress component $\sigma_{zz,P}$) and for a ring-like excitation it is a line load at the coordinate $r = a$ ($\sigma_{zz,R}$, see eq. 3)

$$\sigma_{zz,P}(r) = \sigma_0 \frac{\delta(r)}{2\pi r} \quad , \quad \sigma_{zz,R}(r) = \sigma_0 \frac{\delta(r-a)}{2\pi(r-a)} \quad (3)$$

In transformed domain, this leads to:

$$\sigma_{zz,P}^{H_0}(\xi) = \sigma_0, \quad \sigma_{zz,R}^{H_0}(\xi) = \sigma_0 J_0(a\xi), \quad (4)$$

with the Bessel function of first kind and first order. Further, the methods of Pao and Gajewski [4] can be applied to calculate displacements in the medium or the stress on interfaces can be applied also for a ring-like excitation. The terms just contain an additional $J(a\xi)$. Finally, an integral of the form of equation 5 has to be solved.

$$I = \int_0^{\infty} F(\xi) e^{-j\sqrt{k^2 + \xi^2}z} J_0(r\xi) J_0(a\xi) \xi d\xi \quad (5)$$

$F(\xi)$ contains source and receiver functions depending on the position of the source and if there are calculated displacements or stresses inside a medium or on an interface. Pao and Gajewski used the Cagniard-de Hoop method to solve this integral. But here the approach of Miller-Persey [5] using a steepest descent approximation for the integral is applied. The naïve idea to apply the method directly by substituting $F^*(\xi) = F(\xi) J_0(r\xi)$ fails directly because this would result in a epicenter at the origin, but the epicenter has to be at the coordinate $r = a$. A less common expression of the Bessel function (eq. 6) is needed instead.

$$J_0(r\xi) = \frac{1}{2\pi} \int_0^{\infty} \frac{1}{\sqrt{jx^2 + 2r\xi}} e^{-x^2 - jr\xi} dx + \frac{1}{2\pi} \int_0^{\infty} \frac{1}{\sqrt{jx^2 - 2r\xi}} e^{-x^2 + jr\xi} dx \quad (6)$$

This form is used for both Bessel functions so their product results in a sum of two integrals:

$$I = \frac{1}{\pi} \int_{-\infty}^{\infty} \frac{F(\xi)}{2\xi\sqrt{ar}} e^{-pz + j(r+a)\xi + \frac{\pi}{2}\xi d\xi} + \frac{1}{\pi} \int_{-\infty}^{\infty} \frac{F(\xi)}{2\xi\sqrt{ar}} e^{-pz + j(r-a)\xi + \frac{\pi}{2}\xi d\xi} \quad (7)$$

So the lower term describes the wave from the coordinate $r = a$. and the upper term the wave from $r = -a$. This corresponds to the arrival times of the first and last waves as discussed in the following section. For each term, the steepest descents approximation can be applied [MP].

$$I_1 = \frac{F(\xi_s) \cos\alpha}{\sqrt{2\pi k R a (R \sin(\alpha) - a)}} e^{-jkR} + \frac{F(\xi'_s) \cos\beta}{\sqrt{2\pi k R' a (R' \sin(\beta) + a)}} e^{-jkR} \quad (8)$$

with the wave number k and

$$R = \sqrt{(r-a)^2 + z^2}, \quad R' = \sqrt{(r+a)^2 + z^2},$$

$$\alpha = \arctan\left(\frac{r-a}{z}\right), \quad \beta = \arctan\left(\frac{r+a}{z}\right);$$

$$\xi_s = k \sin(\alpha), \quad \xi'_s = k \sin(\beta) \quad (9)$$

These formulas are implemented and the resulting field is compared with the corresponding one, gained by a point source synthesis. The results are shown in figure 1. Obviously, both fields disagree. The reason is, that the two Bessel functions had been approximated linearly and that the resulting deviation becomes too high. So an alternative approach is proposed:

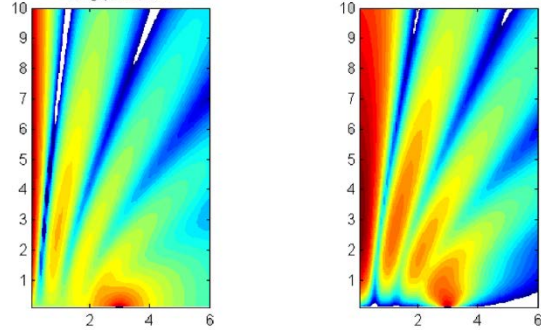


Fig. 1. Comparison of sound fields of a point source at $r = 3$ mm: calculated via the steepest descent approximation for the ring (left) and via point source synthesis (right).

III. APPROACH USING GREEN'S FUNCTIONS OF POINT SOURCES

Equation 10 gives the general form of a Greens function in frequency domain G^ω and in time domain G^δ

$$G^\omega = \frac{S(\phi)}{2\pi R} e^{jkR}, \quad G^\delta = \frac{S(\phi)}{2\pi R} \delta\left(t - \frac{R}{c}\right) \quad (10)$$

R is the distance between source and observation point, S is the directivity pattern, determined by the boundary conditions and the excitation type, ϕ is the angle between R and the surface normal and c the sound velocity of the medium, longitudinal or transversal with the corresponding directivity pattern. Further, δ is the Dirac delta function. This describes the pulse response of on point, e.g. on a ring. To determine the pulse response of a ring-like line force a special convolution is necessary. Equation 11 calculates the sound pressure for a ring with $r = a$ at an observation point $P(x, \theta, z)$ see figure 2.

$$p(x, \theta, z) = \int_0^\pi \frac{a p_0 S(\phi)}{\pi \sqrt{x^2 + a^2 + z^2 - 2x a \cos(\alpha)}} \delta\left(t - \frac{\sqrt{x^2 + a^2 + z^2 - 2x a \cos(\alpha)}}{c}\right) d\alpha \quad (11)$$

Due to the properties of the Dirac delta function, this integral can be solved by substituting

$$t' = \frac{\sqrt{(x^2 - 2x a \cos(\alpha) + a^2 + z^2)}}{c} \quad (12)$$

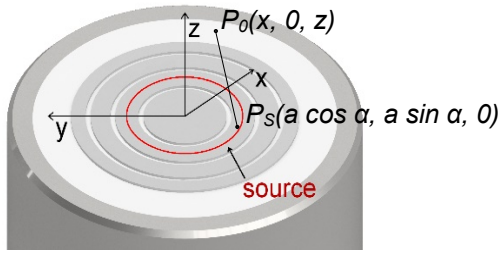


Fig. 2. Array with a ring source

Using the step function $H(t)$ gives:

$$p(x, z) = \frac{2ap_0S(\varphi)(H(t - t_1) - H(t - t_2))}{\pi\sqrt{4x^2a^2 - (x^2 + a^2 + z^2 - c^2t^2)^2}} \quad (13)$$

Where t_1 and t_2 are the arrival times of the partial waves starting from the points on the ring being nearest respectively furthest from the observation point. This supports the thesis discussed below equation 7 that the integral for the inverse Hankel transform needs two epicenters.

$$t_1 = \frac{\sqrt{(x^2 - 2xa + a^2 + z^2)}}{c} \quad (14)$$

$$t_2 = \frac{\sqrt{(x^2 + 2xa + a^2 + z^2)}}{c}$$

Additionally, the pressure on the acoustic axis is determined by:

$$p(0, z) = \frac{p_0S\left(\arccos\left(\frac{z}{ct}\right)\right)\delta\left(t - \frac{\sqrt{a^2 + z^2}}{c}\right)}{\pi\sqrt{a^2 + z^2}} \quad (15)$$

To qualify the algorithm the emitted signals from a disk shaped source are calculated by covering it with ring sources. Figure 3 shows that they are similar to the analytic solution.

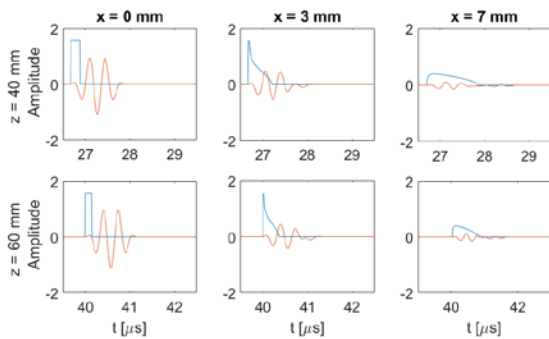


Fig. 3. Calculated signals for a disc source of $d = 10$ mm diameter for different depths (40 mm upper line and 60 mm lower line) and for different radial coordinates r ; left: on acoustic axis, center: out of axis $r < d/2$, right: $r > d/2$; in blue: pulse response; red convolution with a signal of 3 periods with 3 MHz center frequency.

To determine the necessary density of rings, figure 4 shows a detailed comparison for different densities. It shows that the distance between two rings must not be bigger than $2 \mu\text{m}$.

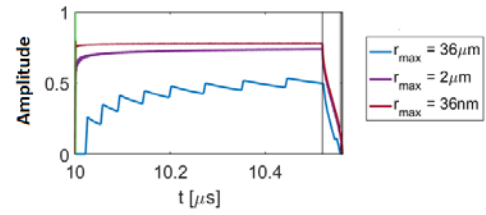


Fig. 4. Calculated signals for a disc source of diameter $d = 10$ mm for different densities of ring sources

IV. APPLICATION TO CALCULATE UNCERTAINTY DURING TEMPERATURE MONITORING IN TISSUE PHANTOMS

A method to monitor the temperature in tissue phantoms has been developed towards a temperature monitoring in tissue during a hyperthermia cancer therapy. It works by evaluating the echoes of small scatterers and allows an exact determination of local speed of sound instead of just evaluating relative changes as with conventional echo shift techniques. To measure the sound velocity and distance to a scatterer, synthetic focusing is applied and the assumed sound velocity as well as the corresponding focus position are varied. Analyzing the resulting signal amplitude gives a maximum if the correct sound velocity is used for focusing. A detailed description and measurement results are given in [6]. This contribution examined the reachable accuracy via simulated data.

Assuming a reflector at a depth $z = 40$ mm in a medium with $c = 1500$ m/s. As mentioned, only the time of flight ($53 \mu\text{s}$) to this reflector can be measured. For synthetic focusing, arbitrary sound velocities can be assumed. For 1000 m/s the corresponding assumed depth for calculating the time lags would be $26,7$ mm. Figure 5 shows the resulting pressure on the acoustic axis (z) for different focusing modes ($F(c_{Fok}, z_{Fok})$)

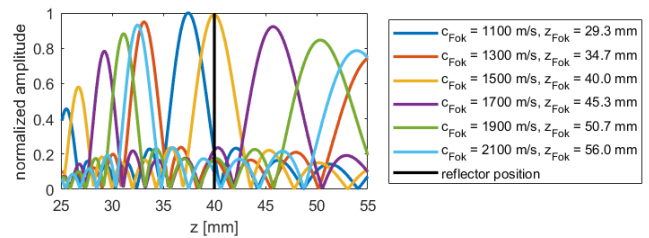


Fig. 5. Pressure on the acoustic axis for different focussion modes

For each focusing regime, the amplitude at the reflector position (40 mm, black line) is detected. It becomes much smaller if the assumed sound velocity differs from the sound velocity in the medium. Figure 6 shows the resulting signal amplitude as a function of the assumed sound velocity used for focusing. Qualitatively the resulting curve agrees very well with the measured one presented in [6].

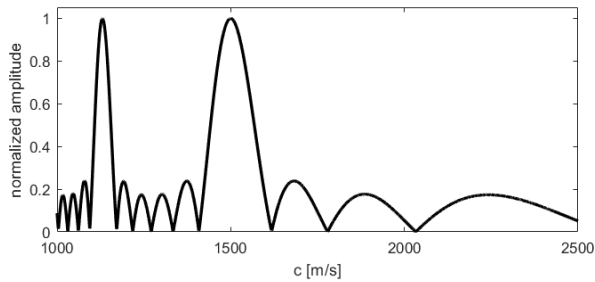


Fig. 6. Resulting amplitude of reflected signal as a function of assumed sound velocity

The same curves are calculated by simulation for each reflector position. Figure 7 shows the amplitude of reflected signal (color-coded) as a function of the reflector position and of the sound velocity used for focusing.

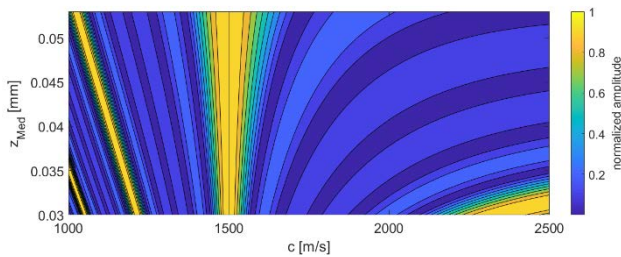


Fig. 7. Resulting amplitude of reflected signal as a function of assumed sound velocity and of reflector position z_{Med}

Taking into account the signal to noise ratio of the measuring system of about 40 dB, the simulation can be used to determine the uncertainty of the measurements. So it cannot be distinguished between values bigger than 99% of the maximum. The resulting uncertainty as a function of measurement depth is shown in figure 8.

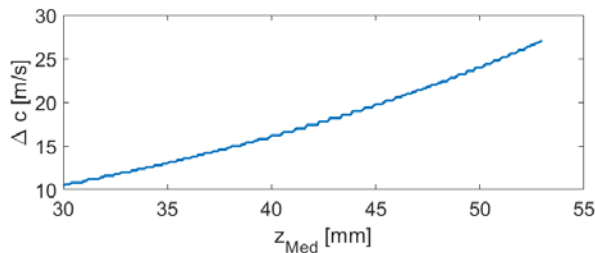


Fig. 8. Resulting amplitude of reflected signal as a function of assumed sound velocity and of reflector position z_{Med}

As expected, the uncertainty increases with the measurement depth due to the increase of the focus area for focusing into greater depths. Furthermore, this result confirms the experimentally determined uncertainty of 2%.

V. CONCLUSION

This contribution presented a new algorithm which allows a fast simulation of the wave propagation in radial symmetric structures. For this, approximated Greens functions for a ring-like excitation are derived. The algorithm is qualified by

comparative calculations for the emitted signals of a disc shaped sound source.

The algorithm can be used to reproduce measurement processes and so to find effective evaluation algorithm, to validate measurement results or to enhance the measurement accuracy.

An example for measuring the longitudinal wave speed in tissue phantoms is given and the evaluation process is modelled. The results can be used to evaluate alternative focusing regimes which should result in an increased accuracy.

VI. ACKNOWLEDGMENT

The authors would like to thank the Deutsche Forschungsgemeinschaft (DFG) for financial support in the project: 260366138.

REFERENCES

- [1] E. Kühnicke, "Three - dimensional waves in layered media with nonparallel and curved interfaces: A theoretical approach." *The Journal of the Acoustical Society of America* 100.2 (1996): 709-716.
- [2] E. Kühnicke, "Plane arrays—Fundamental investigations for correct steering by means of sound field calculations." *Wave Motion* 44.4 (2007): 248-261.
- [3] J. Achenbach, "Wave propagation in elastic solids." Vol. 16. Elsevier, 2012
- [4] Y.H. Pao and R. R. Gajewski "The generalized ray theory and transient responses of layered elastic solids." *Physical acoustics*. Vol. 13. Academic Press, 1977. 183-265.
- [5] G. F. Miller and H. Pursey. "The field and radiation impedance of mechanical radiators on the free surface of a semi-infinite isotropic solid." *Proceedings of the Royal Society of London. Series A. Mathematical and Physical Sciences* 223.1155 (1954): 521-541.
- [6] M. Wolf, L. Timmermann, A. Juhrig, K. Rath, E. Leipner, F. Krutz, E. Kühnicke. "Ultrasonic temperature monitoring in tissue phantoms by locally resolved measurement of longitudinal and transverse wave speed," *Proceedings of the 2019 International Congress on Ultrasound, Bruges, 2019, in press*